Performance of Scientific Cameras With Different Sensor Types in Measuring Dynamic Processes in Fluorescence Microscopy

JASMIN JUNG,[1] SIEGFRIED WEISENBURGER,[2] SAHRADHA ALBERT,[1] DANIEL F. GILBERT,[3] OLIVER FRIEDRICH,[3] VOLKER EULENBURG,[4] JOHANNES KORNHUBER,[1] AND TEJA W. GROEMER[1]*

[1]*Department of Psychiatry and Psychotherapy, Friedrich-Alexander-University of Erlangen-Nuremberg, Erlangen 91054, Germany*
[2]*Nano-Optics Division, Max Planck Institute for the Science of Light, Erlangen 91058, Germany*
[3]*Institute of Medical Biotechnology, Friedrich-Alexander-University of Erlangen-Nuremberg, Erlangen 91052, Germany*
[4]*Department of Biochemistry and Molecular Medicine, Friedrich-Alexander-University of Erlangen-Nuremberg, Erlangen 91054, Germany*

INTRODUCTION

Major breakthroughs like confocal microscopy (Pawley, 2006) and live-cell super-resolution imaging (Shroff et al., 2008) advanced fluorescence microscopy to *the* key technology in life science (Goldman, 2005). During the last two decades, progress in both the fluorescent tags and labeling techniques facilitated the study of dynamic processes in biomedical research: however, the development of new fluorophores such as genetically encoded fluorescent proteins (Heim et al., 1995) and functional tags (Glazer and Rye, 1992; Miesenbock et al., 1998) allows for unimagined specificity. However, novel labeling strategies for synthetic dyes employing nanobodies (Ries et al., 2012) or aptamers (Ellington and Szostak, 1990) overcame limitations given by the size of the biological label. Besides the chosen labeling strategy and the microscope objective, the used camera plays a crucial role in fluorescence microscopy for both the quality of the acquired images and their suitability for subsequent quantitative data analysis.

The performance of a scientific camera can, in general, be described by its sensitivity, its dynamic range, the maximum frame rate, and the number of pixels, which determines the field of view and the resolution. Depending on the question asked, one has to choose the appropriate camera type to provide a satisfying answer, as the image properties of various biological experiments differ dramatically, and therefore different camera properties have to be considered. In the following, we list a selection of typical examples in which the properties of the camera limit the experimental read-out:

1. Static localization studies using fluorescence-labeled antibodies (Frischknecht et al., 2008) have the advantage that excitation is only limited by photobleaching. This results in signal strengths which are still detectable with less sensitive cameras, but typically require a large field of view with high spatial resolution, and thus a high number of pixels.
2. In dynamic, that is, time-resolved, localization studies such as vesicle tracking, where transport

Abbreviations: bg, background; BI EM-CCD, back-illuminated electron-multiplying charge-coupled device; CCD: charge-coupled device; EM-CCD: electron-multiplying charge-coupled device; FI EM-CCD, front-illuminated electron-multiplying charge-coupled device; GFP, green fluorescent protein; SBR, signal-to-baseline ratio; sCMOS, scientific complementary metal oxide semiconductor; SNR, signal-to-noise ratio; spH, synaptobrevin-pHluorin; std, standard deviation

*Correspondence to: Teja W. Grömer, Department of Psychiatry and Psychotherapy, Friedrich-Alexander-University of Erlangen-Nuremberg, Erlangen 91054, Germany E-mail: teja.groemer@uk-erlangen.de

Contract grant sponsor: Interdisciplinary Centre for Clinical Research (IZKF), Erlangen.

TABLE 1. Overview over the camera types tested (type, frame rate, quantum efficiency, and typical applications with selected examples)

Camera type	Maximal frame rate at full frame (per s)	Maximal quantum efficiency	Typical applications
sCCD	11	>40%	Epifluorescence microscopy, calcium imaging (Kim et al., 2012); differential interference contrast microscopy, epifluorescence microscopy (Stewart et al., 2011)
CCD	15	N.A.	Differential interference contrast microscopy, epifluorescence microscopy (Peixoto et al., 2009); immunofluorescence (Trazzi et al., 2010)
FI EM-CCD	31	65%	Bright-field optical tracking (Tsai et al., 2011); epifluorescence video microscopy (Welzel et al., 2010)
BI EM-CCD	35	>90%	Atomic force microscopy, total internal reflection fluorescence (TIRF) microscopy (Gumpp et al., 2009); epifluorescence and TIRF video microscopy (Le et al., 2009)
sCMOS	100	57%	Super-resolution microscopy (Saurabh et al., 2012); high-speed in vivo imaging (Tomer et al., 2012)

vesicles are made visible by transfecting cells with fluorescence-tagged proteins (Welzel et al., 2011b), the exposure time has to be cut down to a minimum to achieve maximal temporal resolution, which produces a weaker, and thus less detectable signal. However, such experiments feature a strong fluorescent background (bg) caused by the accumulation of the tagged protein in cellular compartments such as the Golgi apparatus (Ward et al., 2001), lysosomes or endosomes (Lorenzen et al., 2010). Usually, these structures are larger, bear more protein and are thus of a higher fluorescence intensity than single transport vesicles, making it challenging to find settings within the dynamic range that suit the quantification of multiple levels of intensities. Therefore, besides higher sensor sensitivity the emphasis lies on the camera's dynamic range in this kind of measurement.

3. In other time-resolved processes the signal is stationary, but shows local intensity changes, for example, in the analysis of vesicular exocytosis and endocytosis, visualized via styryl dyes (Betz et al., 1992) or pH-dependent fluorophores (Miesenbock et al., 1998). Thus, when studying the kinetics of exocytosis and endocytosis, it is of great importance to use a camera with a large effective dynamic range, which can image even drastic changes in fluorescence intensity (Voglmaier et al., 2006), and good temporal resolution properties at the same time.

However, all these applications have in common that they require a reasonably high SNR (signal-to-noise ratio), which is necessary to discern signal from bg (Sbalzarini and Koumoutsakos, 2005; Stroebel et al., 2010). Visualizing local dynamic processes with suitable probes often produces images of scattered peaks over bg (Prange and Murphy, 1999), that is, areas without measurable signal of interest consisting of noise from different sources (Stroebel et al., 2010). This kind of scattered peak images yields a typical positively skewed distribution of counts (Welzel et al., 2010), in which if the signal is restricted to the minority of pixels, the peak of the intensity histogram corresponds to the bg values, and the slope to the measured signal (Stroebel et al., 2010).

The standard cameras used in live-cell microscopy are of the charge-coupled device (CCD) type or, when used for applications with extremely low light levels, of the EM-CCD (electron-multiplying CCD) type. In a CCD, photoelectron packages that were generated in capacitive bins on the chip, the pixels, are shifted one by one in a line before they reach the readout amplifier. Until now, cameras based on complementary metal oxide semiconductor (CMOS) technology displayed limited performance. After recent progress, scientific CMOS (sCMOS) cameras were introduced in the field of fluorescence microscopy, but rather in the context of super-resolution microscopy. Especially in this field the performance of sCMOS cameras in comparison with the widely used EM-CCDs is intensely discussed (Huang et al., 2011; Long et al., 2012; Quan et al., 2010; Saurabh et al., 2012). An sCMOS chip is a so called active pixel sensor where every pixel combines a photodetector and its own active amplifier. sCMOS cameras typically have smaller pixels and therefore more pixels on a chip with the same size, and since a CMOS is in essence a parallel read-out device, it can achieve higher read-out rates (Table 1).

To find parameters that reasonably describe the performance of a camera, in this study, we tested cameras with five different sensor types, namely one linear CCD, one sCCD (scientific CCD), one front-illuminated EM-CCD (FI EM-CCD), one back-illuminated EM-CCD (BI EM-CCD), and one sCMOS camera. They were compared in different aspects important for imaging static and dynamic processes, that is, SNR, temporal noise, optimal use of the camera's dynamic range and signal-to-baseline ratio (SBR). Thereby, we established a model system for fluorophores exhibiting a positively skewed intensity distribution. Furthermore, the cameras were challenged with a standard technique in neuroscience, that is, imaging exocytosis and endocytosis in hippocampal neurons transfected with a synaptic vesicle protein tagged with a pH-sensitive fluorophore, to evaluate their applicability in measuring multimolecule intensity changes.

MATERIALS AND METHODS

Cell Culture

Hippocampal neuronal cultures were prepared from 1 to 4 days old Wistar rats (Charles River) as described (Welzel et al., 2010). Neurons were transfected with synaptopHluorin under control of a synapsin promoter

(Sankaranarayanan and Ryan, 2000) on DIV3 with a modified calcium phosphate method (Threadgill et al., 1997). Experiments were performed between 25 and 30 days in vitro. For the α-synaptotagmin-CypHer™5E experiments, neurons were incubated in extracellular solution containing the CypHer™ 5E-labeled antibody (1:100) for 1 h at 37°C. Excess antibody was washed away before imaging.

Imaging

Experiments were conducted at room temperature on a Nikon TI-Eclipse inverted epifluorescence microscope equipped with a 60×, 1.2 NA water immersion objective and Perfect Focus System™. Fluorescent dyes were excited by a Nikon Intensilight C-HGFI through excitation filters centred at 482, 520, and 640 nm using dichroic longpass mirrors (cut-off wavelength 488, 532, and 660 nm), respectively. The emitted light passed emission band-pass filters ranging from 500 to 550 nm, 570 to 640 nm, and 660 to 700 nm, respectively (Semrock, Rochester). Five different types of cameras were compared in their ability to detect fluorescence signals: one linear CCD camera (DS-2MBW, Nikon), one sCCD camera (CoolSnap cf, Photometrics); one front-illuminated EM-CCD camera (iXon DU-885, Andor), one back-illuminated EM-CCD camera (iXon DU-897, Andor), one sCMOS camera (Neo, Andor). In all experiments, only the camera was exchanged while the rest of the setup stayed the same. If possible, the cameras were cooled to −70°C (FI and BI EM-CCD) or −30°C (sCMOS), respectively; the CCD and sCCD camera were run at room temperature. Orange fluorescent, carboxylate-modified microspheres with a diameter of 40 nm (FluoSpheres® 540/560, Invitrogen, Karlsruhe) were diluted 1:10,000 in purified water (Milli-Q, EMD Millipore Corporation, Billerica) and sonicated in a water bath for 5 min. Five hundred microliter of the beads suspension were applied onto a coverslip placed in a perfusion chamber. To prevent the fluorescent beads from moving, excessive fluid was discarded and the coverslip surface dried. If possible, pixel binning was used so that pixel sizes were comparable among the different cameras. Of each defined set of parameters, three serial images were recorded. For the live-cell experiments, coverslips were placed into a perfusion chamber (volume = 500 μL) with extracellular medium containing (in mM): 144 NaCl, 2.5 KCl, 2.5 $CaCl_2$, 2.5 $MgCl_2$, 10 Glucose, 10 Hepes, and pH 7.4 (NaOH). Synaptic boutons were stimulated by electric field stimulation (platinum electrodes, 10 mm spacing, 1 ms pulses of 50 mA and alternating polarity); 10 μM 6-cyano-7-nitroquinoxaline-2,3-dione (Tocris Bioscience) and 50 μM D-amino-5-phosphonovaleric acid (D,L-AP5, Tocris Bioscience) were added to prevent recurrent activity. SynaptopHluorin-transfected hippocampal neurons were stimulated with 600 action potentials (APs) at 30 Hz or 200 APs at 20 Hz, respectively. Images were recorded with an exposure time of 200 ms and a gain close to 5, since the previously determined optimal SNR settings could not be used for some cameras due to saturation. Neurons labeled with the CypHer™5E-coupled antibody were imaged with an exposure time of 1 s and a camera gain of 5.

Image Analysis

All images were analyzed using custom-written MATLAB routines (The MathWorks, Natick). Beads were localized using automated peak detection (Sbalzarini and Koumoutsakos, 2005) in images acquired with good SNR and typically an exposure time of 1 s and a gain close to 5. Intensity values were read out at these determined peaks coordinates in all images. Mean peak values for each image were calculated by averaging the pixel values in each region of interest and then averaged over three subsequently recorded images with identical parameters. To get bg intensity values, a region with an area of 0.24 % of the entire image size, which was the largest area that contained no peak-maximum in the visual inspection, was chosen manually from the image with the highest gain and exposure time values.

Signal-to-noise ratio (SNR) was defined as:

$$\frac{\text{peak amplitude}}{\text{std (background)}} \tag{1}$$

with peak amplitude = peak value – bg value.

Used dynamic range was defined as:

$$\frac{\text{intensity(5\% brightest peaks)-intensity(5\% dimmest peaks)}}{\text{intensity range-background}} \tag{2}$$

Temporal noise was defined as:

$$\frac{\text{std (background)}}{\text{background}} \tag{3}$$

SBR was defined as: $\frac{\text{peak amplitude}}{\text{std (baseline)}}$ (Stroebel et al., 2010) with peak amplitude = value during stimulation – baseline (i.e., before stimulation).

Ethics Statement

All animals were handled in strict accordance with good animal practice as defined by the guidelines of the Free State of Bavaria, and all animal work was approved by the Kollegiales Leitungsgremium of the Franz-Penzoldt Zentrum, Erlangen (reference number TS-1/10).

RESULTS

Introducing Fluorescent Microspheres as a Model System for Fluorescence Images with Skewed Intensity Distributions

In live-cell fluorescence microscopy the visualization of fluorescent organelles/structures, for example, synapses, typically produces images showing scattered peaks over bg (Prange and Murphy, 1999), that is, areas with no signal of interest consisting of noise from different sources. This kind of scattered peak image has a characteristic positively skewed distribution of counts (Welzel et al., 2010). If the signal is restricted to the minority of the pixels, the peak of its intensity histogram corresponds to the bg values and the slope to the measured signal (Stroebel et al., 2010). As a model system for a time-resolved process with local intensity changes, we chose triggered exocytosis and endocytosis in neurons transfected with

synaptopHluorin (spH) (Welzel et al., 2011a; Wienisch and Klingauf, 2006). SynaptopHluorin is a fusion protein of the vesicle protein synaptobrevin2 and superecliptic pHluorin, a modified version of GFP (green fluorescent protein). Transfected into cells, pHluorin constructs, in contrast to GFP, emit light only under alkaline conditions, whereas in an acidic environment, their fluorescence is quenched. This means that, tagged to the intraluminal domain of a vesicle protein, they fluoresce only when this vesicle is exocytosed and the, by then, acidic vesicle lumen comes in touch with the extracellular fluid of a pH of 7.4. Upon endocytosis and subsequent reacidification the fluorescence is quenched again, and thus the variation of fluorescence intensity mirrors the kinetics of exocytosis and following vesicle reuptake. Intensity histograms of images of spH-transfected cells (Fig. 1a) show a typical positively skewed distribution (Fig. 1b), as well as the difference image (Figs. 1e and 1f) that can be calculated by subtracting the fluorescence intensity before electrical stimulation (T_1) from the peak intensity measured at the end of the stimulation (T_2) (Fig. 1c). Figure 1d shows the resulting intensity dynamics, when averaging the intensity of every time point at all peak regions detected in the difference image. Since the peak detection and thus the analysis of the experiment rely on the quality of the difference image, we selected a fluorophore model system that had similar properties as the difference image, but that did not underlie the fluctuations usually occurring in living cells. Fluorescent carboxylate-modified microspheres met these requirements. For imaging, the beads were plated and subsequently dried on cover slips in a high dilution to guarantee they were evenly distributed, which results in images resembling those of the difference images as well as showing a similar intensity distribution in the histogram (Figs. 1g and 1h). As the fluorescent beads exhibit the desired intensity distribution, we can conclude that they can serve as a model system for imaging synapses.

Signal-to-Noise Ratios and Use of Dynamic Range

The fluorescent microspheres were imaged under various conditions, that is, exposure times were altered, and different camera gains were applied if technically possible, to find the best settings for each camera. Since we wanted to compare cameras of different types and thus of quite different sensitivity, the parameters had to be varied over a wide range to meet the requirements of each of the cameras. For direct comparison of the results, image series ($n = 3$) from an individual coverslip were recorded with varying camera parameters. However, this resulted in images without detectable peaks, that is regions of interest, on the one hand, and overexposed images on the other hand. As peaks were stable in location during subsequent measurements, peaks were detected in images with high SNR that did not show saturation artefacts. SNR was then assessed in all other images at these locations. When reading out the total SNR values, that is, the average SNR of all detected peaks in an image, we found the SNR to decline when the images began to saturate, which with the EM-CCD cameras already happened with relatively moderate gain and exposure time settings (Figs. 2k–2o). This is expected as in more and more saturating conditions the bg value still grows while the signal does not. To avoid these estimation

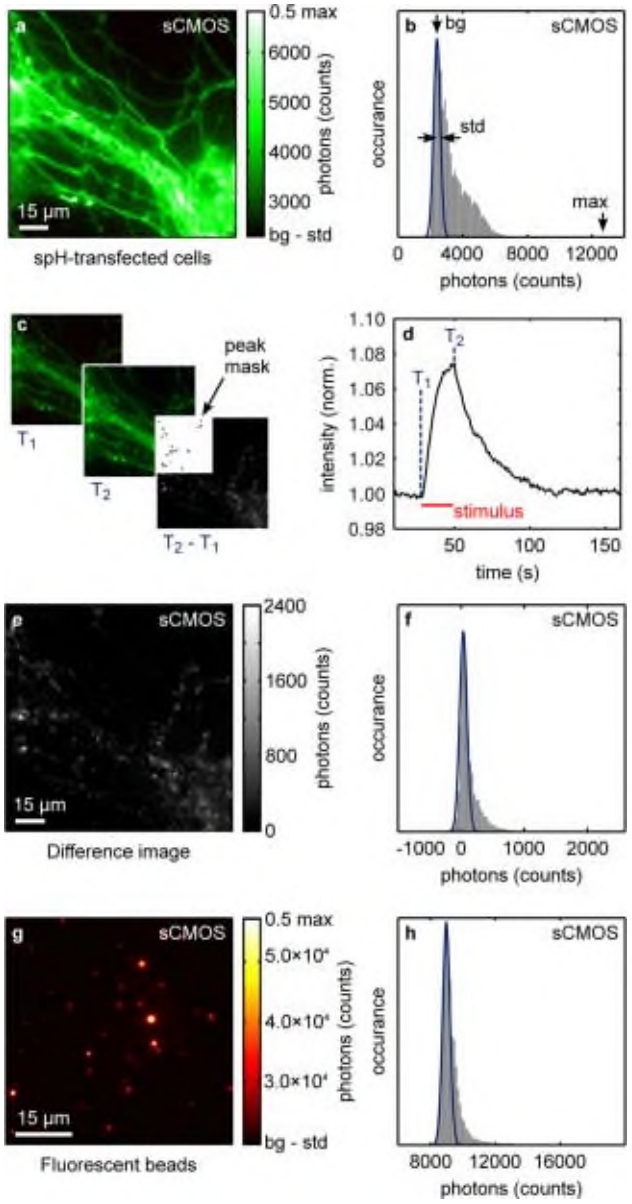

Fig. 1. Fluorescent beads as a model system for fluorescence images of multimolecule spots with skewed intensity distributions. **a**: Cells transfected with synaptopHluorin (spH) were recorded with an sCMOS camera in a video experiment, in which electrical field stimulation evoked changes in fluorescence intensity. **b**: Corresponding intensity histogram. **c**: Scheme of the generation of a difference image by subtracting images acquired before stimulation (T_1) from images acquired at maximal fluorescence intensity (T_2) at the end of the stimulus. Inset: Regions with relevant intensity changes were detected in the difference image via automated peak detection. **d**: Averaged fluorescence intensity kinetics at all regions detected in the difference image. The bar indicates the duration of the electrical stimulus. Fluorescence intensities were normalized to the baseline level before stimulation. **e**: Difference image ($T_2 - T_1$). **f**: Intensity histogram for the difference image. **g**: Fluorescent microspheres recorded with the sCMOS camera. **h**: Intensity histogram for the fluorescent microspheres. [Color figure can be viewed in the online issue, which is available at wileyonlinelibrary.com].

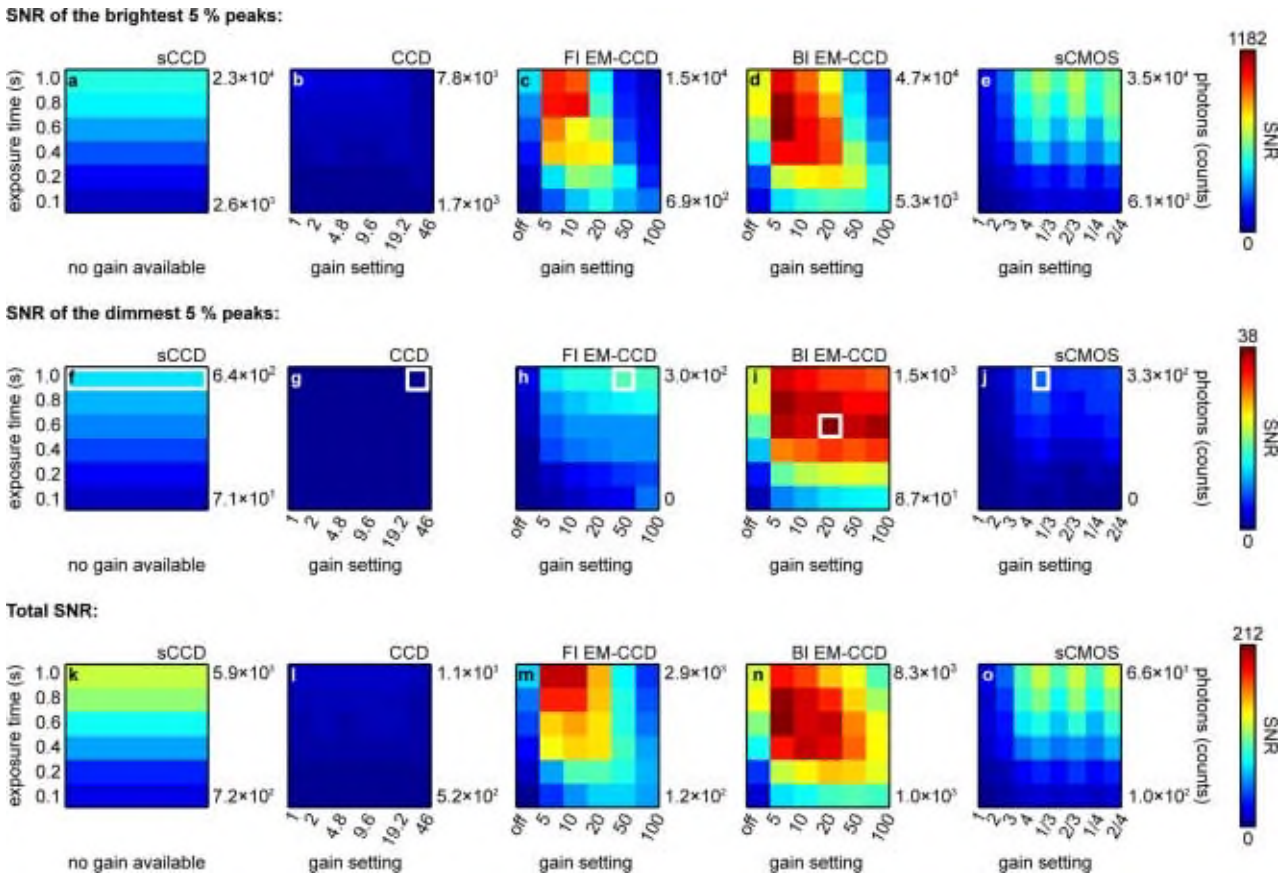

Fig. 2. Relationship between exposure time, gain, and achieved SNR in images of fluorescent beads for different camera types. Fluorescent beads were imaged with different exposure times and camera gains. For all cameras, peaks were detected automatically in high SNR images with the same parameters (Sbalzarini and Koumoutsakos, 2005). Note that the automated peak detection may result in SNR values of 0 or below in low SNR images since SNR values were read out at all peak locations in all images even if there was no peak visible. For each camera SNR values are given as a function of camera gain and exposure time or number of photons, respectively. Maximal and minimal numbers of collected photons per peak are indicated at the right side of each panel. SNR values are color-coded with the colormap ranging from the lowest to the highest SNR value achieved with one of the cameras within the respective fraction of peaks. **a–e**: Mean SNR values of the brightest 5% of the peaks for the individual cameras. **f–j**: Mean SNR values of the dimmest 5% of the peaks for the individual cameras. White box: best SNR. For absolute values see figure 3. **k–o**: Mean SNR values of all detected peaks for the individual cameras. [Color figure can be viewed in the online issue, which is available at wileyonlinelibrary.com.]

errors due to peak values at saturation, we decided to differentiate between peaks that were saturated at high exposure times (brightest 5%, Figs. 2a–2e) and peaks that were never saturated in any of the images (dimmest 5%, Figs. 2f–2j). The nonsaturated peaks were now readily comparable between different cameras. Among these peaks, we figured out the parameters with which each camera could achieve the highest SNR values and thus produced the best images (Figs. 3a–3e): 1 s exposure time for the sCCD (no gain selectable), 1 s and gain 46 for the CCD, 1 s and gain 50 for the FI EM-CCD, 600 ms and gain 20 for the BI-EMCCD, and 1 s and gain 4 for the sCMOS (Figs. 2f–2j). The best signal-to-noise ratio defined as peak amplitude, that is, peak value minus baseline value, divided by the standard deviation of the bg, differed significantly between the cameras tested (Kruskal-Wallis-Test: $P = 0.0156$). The BI EM-CCD featured the best SNR with a value of 38.05 (std = 1.01), followed by the FI EM-CCD with an SNR of 17.20 (std = 1.10) and the sCCD with a value of 13.01 (std = 0.60). In this test the sCMOS achieved an SNR value of 6.02 (std = 1.03), whereas the best SNR of the 5% dimmest peaks detected in the CCD images remained < 1 (Fig. 3f).

Fluorescence markers for dynamic processes require a camera which is highly sensitive and which can detect strong changes in intensity at the same time. When imaging the fluorescent beads with the settings that had led to the best SNR values, we found that the FI EM-CCD camera and the CCD already used 80.58 % and 100 % of their dynamic range, respectively, which, in case of spH-transfected cells, meant that the camera would not be able to detect any larger increases in fluorescence intensity anymore, but would still need the parameters set to achieve a reasonably high SNR. While the sCCD and the BI-EMCCD for best SNR used 63.33 % and 56.13 %, respectively, the sCMOS only used 9.39 % (Fig. 3g). Consequently, the percentage of the dynamic range used at these parameters differed significantly between the cameras (Kruskal-Wallis-Test: $P = 0.0011$).

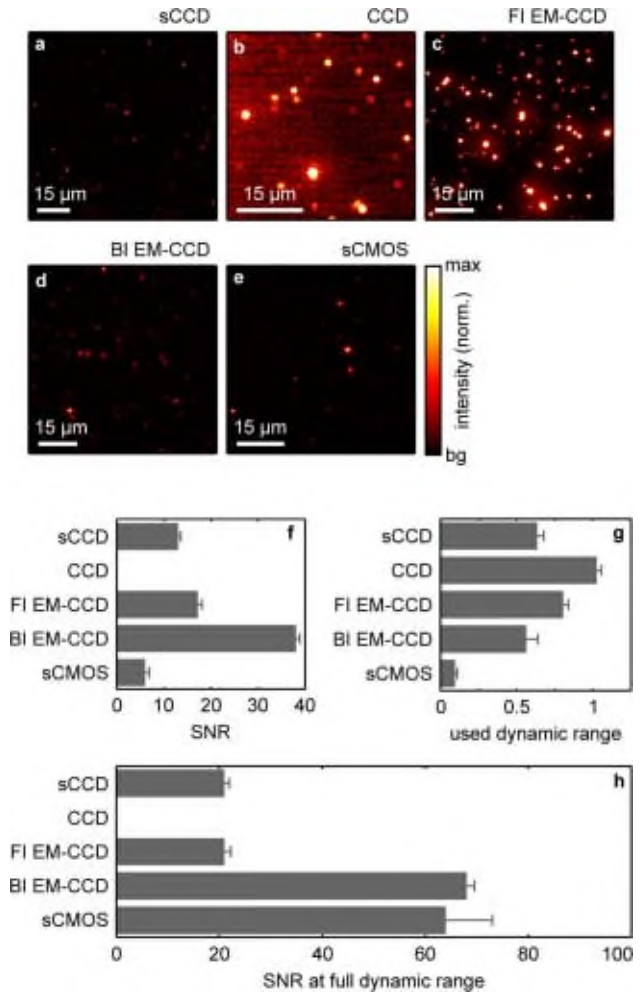

Fig. 3. Quantification of the cameras' SNR values and dynamic range use in images of fluorescent beads. **a**–**e**: Images of fluorescent beads recorded at best SNR settings for the dimmest 5% of the peaks of the individual cameras (see Fig. 2). Fluorescence intensities were normalized, thus ranging from the calculated bg value to the maximally measured value in each image. **f**: Best SNR values of the dimmest peaks as determined in Figures 2f–2**j** vary significantly between the cameras. Kruskal-Wallis-Test: $P < 0.01$. Error bars represent standard deviations. **g**: Usage of the effective dynamic range at best SNR settings for the dimmest peaks varies significantly between the cameras. Kruskal-Wallis-Test: $P < 0.01$. Error bars represent standard deviations. **h**: SNR values at full dynamic range vary significantly. Kruskal-Wallis-Test: $P < 0.05$. SNR at full dynamic range was defined as SNR divided by the fraction of the dynamic range used. Error bars represent standard deviations. [Color figure can be viewed in the online issue, which is available at wileyonlinelibrary.com.]

Resulting from these findings, we calculated the SNR that could be maximally achieved, that is, if it were possible to use the camera's full dynamic range, by dividing the SNR at best settings by the fraction of the dynamic range which was used with these settings. Regarding this parameter, we found the cameras' performance to vary significantly, too (Kruskal-Wallis-Test: $P = 0.0157$). While the CCD featured a value of 0 (std = 0.002), the sCCD achieved an SNR of 20.54 (std = 0.01) and the FI EM-CCD an SNR of 21.40 (std = 0.01). The sCMOS and the BI EM-CCD reached by far the best values of 64.11 (std = 0.09) and 67.79 (std = 0.01), respectively (Fig. 3h).

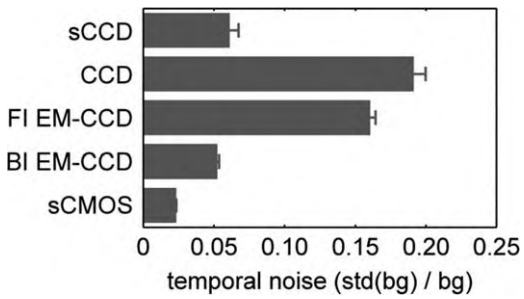

Fig. 4. Quantification of the cameras' temporal noise properties. Temporal noise values at best SNR settings for the dimmest peaks vary significantly between the cameras. Kruskal-Wallis-Test: $P < 0.01$. Temporal noise was defined as standard deviation of the bg normalized to mean bg values. Error bars represent standard deviations.

Temporal Noise Properties

An important feature of cameras used in live-cell imaging is their temporal noise, as minor changes in signal intensities might get lost when the fluctuation between two subsequent images is too strong. To analyze this parameter, we defined temporal noise as the standard deviation of the bg divided by the mean bg intensity of three serial images. When we calculated the temporal noise value for the images with the best SNR (settings: see chapter "Signal-to-noise ratios and use of dynamic range"), we found that the temporal noise varied significantly between the cameras (Kruskal-Wallis-Test: $P = 0.0011$), and that the sCMOS exhibited the lowest relative temporal noise with a value of 0.02 normalized std (bg; std = 3.0×10^{-5}). While the sCCD and the BI EM-CCD featured values still in the same range [0.04 (std = 0.0061) and 0.03 (std = 0.0013), respectively], the temporal noise of the FI EM-CCD and the CCD with values of 0.09 (std = 0.0038) and 0.25 (std = 0.0085) was much higher (Fig. 4). Interestingly, when expressing the temporal noise as a function of the gain, we found the temporal noise of the EM-CCDs and the sCMOS to increase exponentially [R^2 (FI EM-CCD) = 0.98; R^2 (BI EM-CCD) = 0.91; R^2 (sCMOS) = 0.92), whereas the temporal noise of the CCD camera stayed almost constant (Supporting Information Fig. S1).

Performance in Dynamic Measurements

For the live-cell experiments, synaptopHluorin-transfected hippocampal neurons (Figs. 5a–5d) were excited via electrical field stimulation with 600 APs at a rate of 30 Hz or 200 APs at a rate of 20 Hz, respectively. The resulting increase in fluorescence intensity (Supporting Information Fig. S2) was captured with an exposure time of 200 ms and approximately the same gain (5, if possible) for all cameras, as best SNR settings were not applicable due to saturation. From the resulting intensity kinetics curve (Fig. 1d), the SBR was calculated by dividing the peak amplitude (i.e., the baseline value, T_1, subtracted from the peak value, T_2) by the standard deviation of the baseline value. Similar to the data analysis in the model system, the SBR at full dynamic range was calculated by dividing the SBR by the used dynamic range. The CCD camera featured values of 632.14 (std = 25.11) for the 600 AP stimulus or 630.35 (std = 25.28) for the 200

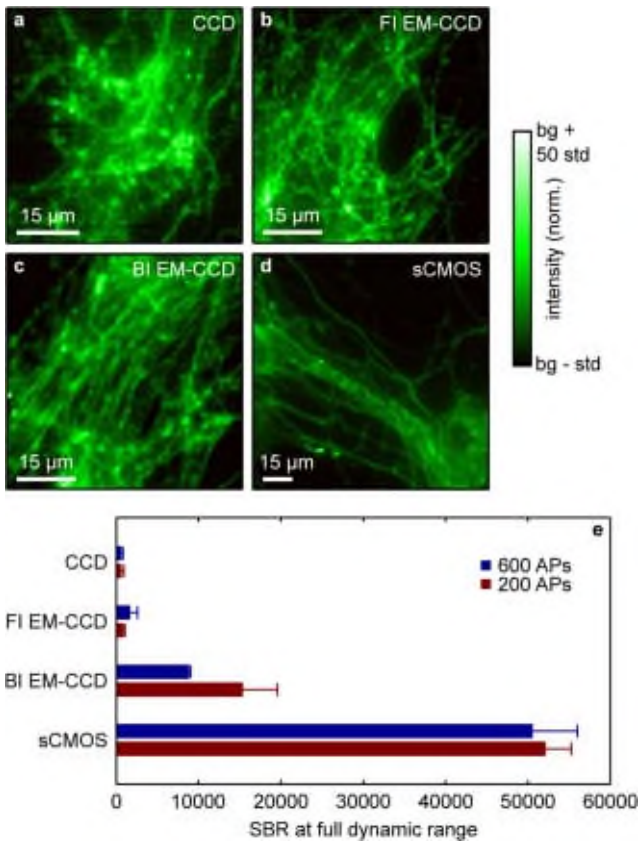

Fig. 5. The cameras' performance in dynamic measurements with living cells. **a**–**d**: Images of spH-transfected cells in a video experiment before electrical stimulation recorded with different cameras. For comparability, cells were imaged using the same exposure times and approximately the same camera gain settings. **e**: SBR values at full dynamic range vary significantly between the cameras, both for the 200 and the 600 AP stimulus. Kruskal-Wallis-Test: $P < 0.05$. SBR at full dynamic range was defined as SBR divided by the fraction of the dynamic range used. Error bars represent standard deviations. [Color figure can be viewed in the online issue, which is available at wileyonlinelibrary.com.]

AP stimulus, respectively, while the FI EM-CCD achieved SBRs at full dynamic range of 1,790.95 (600 AP, std = 903.87) and 902.20 (200 AP, std = 73.47). However, the BI EM-CCD and the sCMOS camera reached higher values of 10,964.12 (600 AP, std = 4,077.73) and 19,187.09 (200 AP, std = 9,636.96) or even 50,881.98 (600 AP, std = 9,250.51) and 53,216.58 (200 AP, std = 8,828.05), respectively. Thus, the cameras' SBR at full dynamic range differed significantly between the cameras, both for the strong and the weak stimulus (Kruskal-Wallis-Test: $P = 0.0156$).

To test another fluorophore with a different wavelength and to provide data on static measurements in living cells, we stained hippocampal neurons with an antibody against synaptotagmin1 labeled with a modified Cy5 variant (CypHer™ 5E), which is quenched in basic, but fluorescent in acidic environments, and thus works just the opposite way as spH (Adie et al., 2002). Here, we incubated the cells with the antibody which binds to synaptotagmin1 when the protein is presented on the cell membrane after spontaneous exocytosis. After compensatory endocytosis the antibody is then localized in the acidic synaptic vesicles, and because of its now fluorescent state another tool to label synapses (Supporting Information Fig. S3a-c). We compared the maximally achievable SNR values (see "Signal-to-noise ratios and use of dynamic range") and found them to differ significantly (Kruskal-Wallis-Test: $P = 0.0273$). Whereas the sCMOS featured the best SNR value of 13,766.43 (std = 462.48), the BI EM-CCD camera with a value of 9,198.32 (std = 580.46) was still superior to the FI EM-CCD camera (SNR = 380.60, std = 35.30) (Supporting Information Fig. S3d).

DISCUSSION

Recent work (Huang et al., 2011; Long et al., 2012; Quan et al., 2010) has proven that finding the appropriate sensor type for a certain experimental setup is a hotly debated issue. Here, we sought to determine different camera parameters important in quantitative dynamic live-cell measurements and to present a methodology to assess the suitability of different camera types for this kind of experiment.

To reproducibly assess the parameters mentioned above in our experiments, we established a model system for imaging synapses and other assays producing scattered peaks over bg. We showed that fluorescent microspheres resemble these fluorescently labeled structures in their fluorescence characteristics, that is, a positively skewed intensity distribution.

Obviously, the parameter of the greatest importance in camera performance in both static and dynamic measurements is the signal-to-noise ratio, as a reasonably high SNR is necessary for the signal of interest to be detected at all. In terms of the SNR, the EM-CCD cameras are still superior to the other sensor types. The reason for this is the higher quantum efficiency of EM-CCD sensors leading to a better signal strength and therefore to higher SNR values (Fig. 3f). However, in the nonsingle molecule situations depicted here, the EM-CCD could not be operated with the EM gain settings that would allow for the lowest readout noise without saturating.

When it comes to the measurement of changes in fluorescence intensity, it depends on the experimental design whether the camera's effective dynamic range or the temporal noise is the important parameter. Here, we found the sCMOS to be at an advantage, both at coping with drastic changes in intensity (Fig. 3g) and at detecting only subtle fluctuations (Fig. 4). Additionally, in fast dynamic processes, the maximal achievable frame rate and therefore time resolution might also be of interest (Table 1). Due to its design, an sCMOS camera will generally be faster than an EM-CCD camera as explained above. Nevertheless, the sCMOS' SBR in the dynamic measurements conducted is, similar to the static SNR measurement, lower compared to the SBR of the EM-CCD cameras. However, when putting the SNR or the SBR, respectively, in a relation to the dynamic range used to achieve this SNR/SBR, the sCMOS is at a great advantage (Fig. 5e). Therefore, if the sCMOS were employed in an experimental setting in which the camera's full dynamic range can be used, the sCMOS would be an optimal tool to image structures of lowest intensity or intensity changes. In dynamic measurements, this is of course limited by the high temporal resolution required,

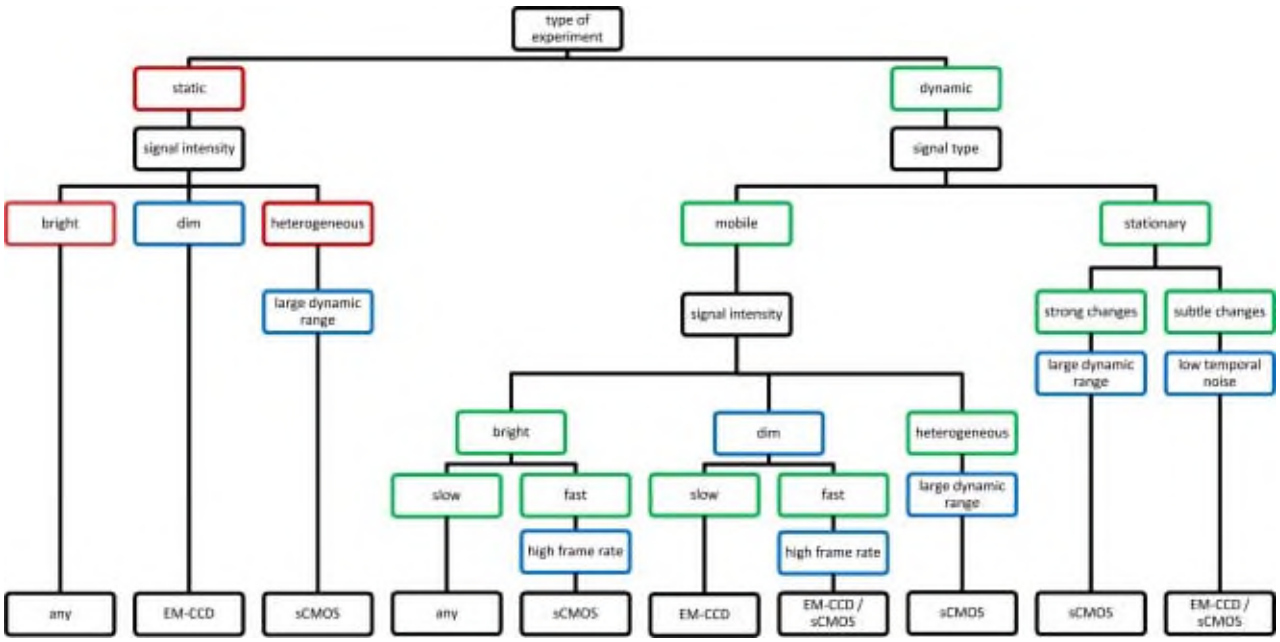

Fig. 6. Decision tree. Guidelines with which the appropriate sensor type can be found. Experiments with a static signal can be distinguished from dynamic measurements. Latter can be further classified in recordings with mobile signals and stationary signals whose intensity changes over time. Red boxes: static measurements; green boxes: dynamic measurements; blue boxes: parameters of special interest. [Color figure can be viewed in the online issue, which is available at wileyonlinelibrary.com.]

though. Other crucial features of a camera are its spatial resolution and a large field of view, determined by its pixel per chip size ratio, which is very important in localization studies. Clearly, a higher resolution is of advantage, but the signal strengths of the objects observed and the camera's quantum efficiency set a limit to this.

In Figure 6 we present a possible approach how to systematically classify a (biological) experiment in terms of its requirements on an appropriate sensor type. When following this decision tree it becomes clear that there are only a couple of parameters that decide which camera type might be suitable for a certain experiment. Among these some are of special importance, that is, the ability to detect even signals of low intensity, the dynamic range, the frame rate, and the temporal noise properties. This is because these parameters limit the choice mostly to a single sensor type, for example, in the case of a high frame rate to the sCMOS camera. Conclusively, we found that in terms of SNR, the EM-CCD cameras are still superior to the sCMOS cameras due to the higher quantum efficiency and therefore better suited for low light conditions such as single-molecule measurements. However, the higher dynamic range of the sCMOS compared with the EM-CCD cameras makes it the camera of choice when either confronted with signals that drastically change their intensity over time, when it is necessary to avoid saturation due to both low intensity and high intensity features in an image, or in experimental setups that allow for an optimal usage of its dynamic range. These are typical situations in multi-molecule measurements that in terms of scientific advance by far outnumber single-molecule measurements in life sciences.

ACKNOWLEDGMENTS

The authors thank Katrin Ebert for excellent technical support.

REFERENCE

Adie EJ, Kalinka S, Smith L, Francis MJ, Marenghi A, Cooper ME, Briggs M, Michael NP, Milligan G, Game S. 2002. A pH-sensitive fluor, CypHer 5, used to monitor agonist-induced G protein-coupled receptor internalization in live cells. Biotechniques 33:1152-1154, 1156-1157.

Betz WJ, Mao F, Bewick GS. 1992. Activity-dependent fluorescent staining and destaining of living vertebrate motor nerve terminals. J Neurosci 12:363-375.

Ellington AD, Szostak JW. 1990. In vitro selection of RNA molecules that bind specific ligands. Nature 346:818-822.

Frischknecht R, Fejtova A, Viesti M, Stephan A, Sonderegger P. 2008. Activity-induced synaptic capture and exocytosis of the neuronal serine protease neurotrypsin. J Neurosci 28:1568-1579.

Glazer AN, Rye HS. 1992. Stable dye-DNA intercalation complexes as reagents for high-sensitivity fluorescence detection. Nature 359:859-861.

Goldman RD, Spector D. 2005. Live Cell Imaging: A Laboratory Manual. Cold Spring Harbor, New York: Cold Spring Harbor Laboratory Press.

Gumpp H, Stahl SW, Strackharn M, Puchner EM, Gaub HE. 2009. Ultrastable combined atomic force and total internal reflection fluorescence microscope [corrected]. Rev Sci Instrum 80:063704.

Heim R, Cubitt AB, Tsien RY. 1995. Improved green fluorescence. Nature 373:663-664.

Huang ZL, Zhu H, Long F, Ma H, Qin L, Liu Y, Ding J, Zhang Z, Luo Q, Zeng S. 2011. Localization-based super-resolution microscopy with an sCMOS camera. Opt Express 19:19156-19168.

Kim JA, Han E, Eun CJ, Tak YK, Song JM. 2012. Real-time concurrent monitoring of apoptosis, #cytosolic calcium, and mitochondria permeability transition for hypermulticolor high-content screening of drug-induced mitochondrial dysfunction-mediated hepatotoxicity. Toxicol Lett 214:175-181.

Le NC, Yokokawa R, Dao DV, Nguyen TD, Wells JC, Sugiyama S. 2009. Versatile microfluidic total internal reflection (TIR)-based devices: Application to microbeads velocity measurement and

single molecule detection with upright and inverted microscope. Lab Chip 9:244-250.
Long F, Zeng S, Huang ZL. 2012. Localization-based super-resolution microscopy with an sCMOS camera Part II: Experimental methodology for comparing sCMOS with EMCCD cameras. Opt Express 20:17741-17759.
Lorenzen A, Samosh J, Vandewark K, Anborgh PH, Seah C, Magalhaes AC, Cregan SP, Ferguson SS, Pasternak SH. 2010. Rapid and direct transport of cell surface APP to the lysosome defines a novel selective pathway. Mol Brain 3:11.
Miesenbock G, De Angelis DA, Rothman JE. 1998. Visualizing secretion and synaptic transmission with pH-sensitive green fluorescent proteins. Nature 394:192-195.
Pawley JB. 2006. Handbook of Biological Confocal Microscopy. Berlin: Springer.
Peixoto PM, Ryu SY, Pruzansky DP, Kuriakose M, Gilmore A, Kinnally KW. 2009. Mitochondrial apoptosis is amplified through gap junctions. Biochem Biophys Res Commun 390:38-43.
Prange O, Murphy TH. 1999. Correlation of miniature synaptic activity and evoked release probability in cultures of cortical neurons. J Neurosci 19:6427-6438.
Quan T, Zeng S, Huang ZL. 2010. Localization capability and limitation of electron-multiplying charge-coupled, scientific complementary metal-oxide semiconductor, and charge-coupled devices for superresolution imaging. J Biomed Opt 15:066005.
Ries J, Kaplan C, Platonova E, Eghlidi H, Ewers H. 2012. A simple, #versatile method for GFP-based super-resolution microscopy via nanobodies. Nat Methods 9:582-584.
Sankaranarayanan S, Ryan TA. 2000. Real-time measurements of vesicle-SNARE recycling in synapses of the central nervous system. Nat Cell Biol 2:197-204.
Saurabh S, Maji S, Bruchez MP. 2012. Evaluation of sCMOS cameras for detection and localization of single Cy5 molecules. Opt Express 20:7338-7349.
Sbalzarini IF, Koumoutsakos P. 2005. Feature point tracking and trajectory analysis for video imaging in cell biology. J Struct Biol 151:182-195.
Shroff H, Galbraith CG, Galbraith JA, Betzig E. 2008. Live-cell photoactivated localization microscopy of nanoscale adhesion dynamics. Nat Methods 5:417-423.
Stewart MP, Helenius J, Toyoda Y, Ramanathan SP, Muller DJ, Hyman AA. 2011. Hydrostatic pressure and the actomyosin cortex drive mitotic cell rounding. Nature 469:226-230.
Stroebel A, Welzel O, Kornhuber J, Groemer TW. 2010. Background determination-based detection of scattered peaks. Microsc Res Tech 73:1115-1122.
Threadgill R, Bobb K, Ghosh A. 1997. Regulation of dendritic growth and remodeling by Rho, Rac, and Cdc42. Neuron 19:625-634.
Tomer R, Khairy K, Amat F, Keller PJ. 2012. Quantitative high-speed imaging of entire developing embryos with simultaneous multiview light-sheet microscopy. Nat Methods 9:755-763.
Trazzi S, Steger M, Mitrugno VM, Bartesaghi R, Ciani E. 2010. CB1 cannabinoid receptors increase neuronal precursor proliferation through AKT/glycogen synthase kinase-3beta/beta-catenin signaling. J Biol Chem 285:10098-10109.
Tsai FC, Tai LA, Wang YJ, Xiao JL, Hsu TH, Yang CS, Lee CH. 2011. Three-dimensional tracking and temporal analysis of liposomal transport in live cells using bright-field imaging. Microsc Res Tech 74:531-538.
Voglmaier SM, Kam K, Yang H, Fortin DL, Hua Z, Nicoll RA, Edwards RH. 2006. Distinct endocytic pathways control the rate and extent of synaptic vesicle protein recycling. Neuron 51:71-84.
Ward TH, Polishchuk RS, Caplan S, Hirschberg K, Lippincott-Schwartz J. 2001. Maintenance of Golgi structure and function depends on the integrity of ER export. J Cell Biol 155:557-570.
Welzel O, Tischbirek CH, Jung J, Kohler EM, Svetlitchny A, Henkel AW, Kornhuber J, Groemer TW. 2010. Synapse clusters are preferentially formed by synapses with large recycling pool sizes. PLoS One 5:e13514.
Welzel O, Henkel AW, Stroebel AM, Jung J, Tischbirek CH, Ebert K, Kornhuber J, Rizzoli SO, Groemer TW. 2011a. Systematic heterogeneity of fractional vesicle pool sizes and release rates of hippocampal synapses. Biophys J 100:593-601.
Welzel O, Knorr J, Stroebel AM, Kornhuber J, Groemer TW. 2011b. A fast and robust method for automated analysis of axonal transport. Eur Biophys J 40:1061-1069.
Wienisch M, Klingauf J. 2006. Vesicular proteins exocytosed and subsequently retrieved by compensatory endocytosis are nonidentical. Nat Neurosci 9:1019-1027.